Bull. Chem. Soc. Ethiop. **2024**, 38(5), 1225-1240.
DOI: https://dx.doi.org/10.4314/bcse.v38i5.3

ISSN 1011-3924
Printed in Ethiopia
Online ISSN 1726-801X

MANGANESE OXIDE-COFFEE HUSK AND KHAT (CATHA EDULIS) LEFTOVER BIOCHAR NANOCOMPOSITES FOR REMOVAL OF Cr(VI) FROM WASTEWATER

Jemere Kochito[1], Olu Emmanuel Femi[2], Tamene Tadesse[1], Negera Abdisa[3] and Abera Gure[1*]

[1]Department of Chemistry, College of Natural Sciences, Jimma University, P. O. Box 378, Jimma, Ethiopia
[2]Faculty of Material Science and Engineering, Jimma Institute of Technology, Jimma University, P. O. Box 378, Jimma, Ethiopia
[3]Department of Chemistry, College of Natural and Computational Sciences, Wollega University, P.O. Box 395, Nekemte, Ethiopia

(Received October 17, 2023; Revised May 6, 2024; Accepted May 11, 2024)

ABSTRACT. This study investigates the use of manganese oxide-biochar-nanocomposites synthesized from coffee husk (CH) and khat leftover (KL) for Cr(VI) removal from water. Two pristine biochars of CH and KL were separately synthesized by pyrolyzing their biomasses at 300 °C for 1 h. Similarly, biochar-based nanocomposites were synthesized by pretreating 25 g of each biomass with 12.5 mmol of $KMnO_4$ and pyrolyzing at 300 °C for 1 h. The pristine biochars, synthesized by pyrolysis of CH and KL, removed 74.98% and 84.78% of Cr(VI) from aqueous solutions containing 20 mg L^{-1}, respectively. However, the resulting nanocomposites exhibited a maximum removal efficiency of 99.63% with manganese oxide-coffee husk biochar nanocomposite (MnO_X-CHBNC) and 99.84% with manganese oxide-khat leftover biochar nanocomposite (MnO_X-KLBNC) of the Cr(VI). The adsorption isotherm fitted well with the Langmuir isotherm, indicating favorable monolayer adsorption. The kinetics of adsorption followed the pseudo-first-order model. The MnO_X-CHBNC and MnO_X-KLBNC demonstrated satisfactory removal efficiencies even up to six cycles, indicating their potential effectiveness for large-scale use in removing Cr (VI) from wastewater.

KEY WORDS: Adsorption, Biochar-nanocomposite, Coffee husk, Cr(VI) removal, Khat leftovers

INTRODUCTION

Emissions of toxic heavy metals from industries such as tanneries, textile, breweries, metallurgy, dyeing factories, and agro-processing contaminate surface water, groundwater, agricultural soils, and food crops, and they cause acute and chronic human health risks to the population through different pathways [1]. Chromium is one of the widespread heavy metals in the environment, considered a priority pollutant by the United States Environmental Protection Agency (US EPA) [2]. Cr exists mainly as Cr(III) and Cr(VI) in the natural environment, while Cr(VI) is much more poisonous, soluble, and mobile than Cr(III). Moreover, Cr(VI) can be absorbed by hydrophytes and leached into groundwater, causing poisonous and harmful effects on humans [3]. Therefore, using appropriate treatment procedures before discharging industrial effluents into the environment is important.

Different physical and chemical techniques such as electrochemical [4], ultrafiltration [5], ion exchange [6], chemical precipitation [7], and coagulation [8] have been used to remove Cr(VI) from wastewater. However, each method has inherent limitations, such as high energy consumption, cost, generation of toxic sludge, incomplete treatment, and high reagent consumption [9]. Among the existing methods, adsorption is a suitable process for removing heavy metal ions from contaminated water because of its low cost, higher removal efficiency, and simple regeneration [10].

*Corresponding authors. E-mail: abera.gure@ju.edu.et

The removal efficiency of heavy metals through adsorption mainly depends on the adsorbent materials [11]. The adsorbents, such as activated carbon, natural clay minerals, synthetic nanomaterials, and biomass, have been employed to remove inorganic and organic contaminants from aqueous solutions. However, some of these adsorbents have limitations like oxidation, aggregation, and the high cost of commercial materials such as activated carbon, zeolite, iron oxides, fullerene, and graphene [2]. Nowadays, scholars are focusing on using activated biochar to overcome some drawbacks associated with activated carbon and commercial adsorbents [12].

Metallic oxide nanoparticles such as magnetic ferric, manganese, titanium, and magnesium oxide have been used in wastewater treatment [13]. Nevertheless, nanoparticle aggregation presents a challenge, necessitating the use of supporting materials to enhance their stability and recyclability [14]. The biochar-based nanocomposite involves the use of composite material that combines the advantages of biochar and nano-materials [15].

Metal salts such as $AlCl_3$, $CaCl_2$, $MgCl_2$, $KMnO_4$, $MnCl_2$, $ZnCl_2$, and $TiCl_4$ are commonly used to activate biochar, resulting in the formation of Al_2O_3, AlOOH, CaO, MgO, MnOx, ZnO and TiO_2 nanoparticles on the biochar surface [16]. Most biochar-based nanocomposites are synthesized by chemical activation using metallic ions. The synthesis can proceed in either one-step or two-step modification processes [15]. In a one-step process, both carbonization and activation are completed simultaneously in the presence of an activator. On the other hand, in a two-step process, the biomass feedstock is carbonized first, followed by treatment with the appropriate salt. The metal ions used for activation attach to the surface or get into the interior of biomass upon impregnating into the metal ion salt solutions. Then, after pyrolysis, the metal ions are transformed into nano-metal oxide/metal hydroxide, and the biomass impregnated with metal ions becomes biochar-based nanocomposites [14].

In Ethiopia, coffee and khat are produced and consumed, which yields tons of biomass waste that pollutes the environment [17]. Unaddressed disposal of coffee husk (CH) and khat (*Catha edulis*) leftovers (KL) increases municipality waste, which leads to increased transportation costs when taken to the disposal area [18]. This study evaluated the conversion of CH and KL into useful products, which have dual advantages. These are removing toxic pollutants from wastewater and disposing of biomass wastes economically. The manganese oxide-coffee husk biochar nanocomposite (MnO_X-CHBNC) and manganese oxide-khat leftover biochar nanocomposite (MnO_X-KLBNC) were produced, characterized, and their Cr(VI) removal efficiencies were evaluated. The effects of contact time, adsorbent dose, initial concentration, and pH on the two adsorbents' Cr(VI) adsorption capacities were studied, and the kinetics and adsorption isotherms were evaluated. The desorption studies of Cr(VI) from the MnO_X-CHBNC and MnO_X-KLBNC were conducted to evaluate the regeneration or reusability of the adsorbents.

EXPERIMENTAL

Chemicals and reagents

The CH samples were collected from coffee pulping industries in Mizan-Aman town and KL samples were collected from Jimma town, both in Ethiopia. These two biomasses were chosen due to their easy availability and the significant amount of municipal solid waste they produce, which causes serious environmental pollution throughout the country.

Various chemicals and reagents such as $KMnO_4$ (99%, Finkem), $K_2Cr_2O_7$ (99%, NICE), HNO_3 (69%, Qualikems Fine Chemicals), KBr (spectroscopic grade), and NaOH (99%, Merck) as well as NaCl (99.5%, Sigma-Aldrich) were used.

Preparation of MnO_X-CHBNC and MnO_X-KLBNC

The KL samples, which included hard leaves, branches and twigs typically discarded by producers, traders and consumers, were cut into small slices. They were then washed with

deionized water, dried at 105 °C for 24 h, milled into powders of 2 mm, and stored in a dry plastic container at ambient conditions [19]. Likewise, the CH samples were cleaned, dried, ground, and stored following the same procedures as the KL sample.

To synthesize biochar nanocomposite (BNC) materials, 25 g of CH and KL powders were separately immersed in a 500 mL beaker containing 300 mL of a 12.5 mmol $KMnO_4$ solution following the procedure reported by Zheng and coworkers [20]. After stirring the content for 1 h, the water content was evaporated to dryness in an oven at 80 °C until the weight of the mixture became constant. The dried sample was transferred to a crucible, covered with aluminium foil, and placed into a Muffle furnace (DDRAWELL Artist of Science Muffle Furnace 1000 °C SX-4-10, Shanghai, China) initially heated to 110 °C. After 30 min, the heating temperature was ramped up at 10 °C min^{-1} until it reached 300 °C for pyrolyzing for 1 h at this temperature. The synthesized biochar-metal oxide/hydroxide composite was then cooled at room temperature, ground and sieved with mesh sizes of 0.1 - 0.2 mm, repeatedly washed with deionized water, oven-dried at 80 °C and kept in a plastic container for further experiments. The prepared pristine and nanocomposites were labelled as coffee husk biochar (CHB), khat leftover biochar (KLB), MnO_X-CHBNC, and MnO_X-KLBNC.

Measurements and characterization

An X-ray diffractometer, XRD (DRAWELL Artist of Science XRD-7000, Shanghai, China), with a Cu tube radiation source, was used for the analysis of the crystallinity of the synthesized materials. The surface chemical functional groups of the materials were investigated using Fourier transforms infrared (FTIR) spectroscopy (Spectrum 65 FT-IR, PerkinElmer) in the region of 4000-400 cm^{-1}, at a resolution of 4 cm^{-1} in a solid state with KBr. Surface morphologies of the materials were characterized by scanning electron microscopy, and SEM (FEI QUANTA 250, Romania). A multipoint Brunauer-Emmett-Teller (BET) method using ASAP 2020 surface area and porosity analyzer (ASAP 2020, Micromeritics, USA) via nitrogen adsorption at 77 K was used for analyzing surface area, and porosity of the adsorbents. A double-beam UV-Vis spectroscopy (SPECORDR200 PLUS, Analytik Jena, Germany) was used for quantitative Cr(VI) analysis.

Batch adsorption studies

Preliminary adsorption tests were conducted to evaluate the removal efficiencies of CHB, KLB, MnO_X-CHBNC, and MnO_X-KLBNC for Cr(VI) from an aqueous solution using the procedure described in the literature [21]. Batch experiments were conducted to evaluate the rate and adsorption equilibrium phenomena related to Cr(VI) adsorption.

During the analysis, five concentrations of Cr(VI) were prepared by diluting the 1000 mg L^{-1} stock standard solution of Cr(VI) that had been previously prepared by dissolving 2.83 g of $K_2Cr_2O_7$ in deionized water [22]. To conduct the isotherm studies, a solution containing initial Cr(VI) concentrations ranging from 10 to 100 mg L^{-1} was mixed with 0.10 g of the adsorbent materials. The kinetics were studied using initial concentrations of 20, 100, and 300 mg of Cr(VI) at pH 2, using 0.1 g of each MnO_X-CHBNC and MnO_X-KLBNC separately. After shaking the mixture on the horizontal shaker at 200 rpm, the content was filtered using Whatman filter paper. Then, 1 mL of DPC solution, which had been prepared earlier by dissolving 0.25 g of DPC in 50 mL acetone and diluting to 100 mL with deionized water [23], was added to the filtrate and kept for 10 min. The absorbance of the solutions was then determined using a UV-Vis spectrophotometer at the monitoring wavelength of 540 nm.

The Cr(VI) removal efficiency (R) for each adsorbent was calculated using Equation 1, and the adsorption capacity (q_e) was determined employing Equation 2.

$$R = \frac{(C_o - C_e)}{C_o} x100 \quad (1)$$

$$q_e = \frac{(C_o - C_e)V}{m} \quad (2)$$

C_o (mgL^{-1}) and C_e (mgL^{-1}) are the initial and equilibrium adsorbate concentrations, respectively; m (g) is the mass of the adsorbent, and V (L) is the volume of the adsorbate solution [24].

Reusability of the adsorbents

To evaluate the reusability of the adsorbents, six cycles of consecutive adsorption-desorption were carried out at 25 ℃ [25]. For each cycle, adsorption was conducted by shaking 2 g of each MnO_X-CHBNC, and MnO_X-KLBNC dispersed in 250 mL of Cr(VI) solution with an initial concentration of 20 mg L^{-1} for 120 min at pH 2. For desorption, Cr(VI) loaded adsorbent was dispersed in 100 mL of 0.1M KOH, shaken for 120 min, and separated by filtration. After each adsorption-desorption cycle, the MnO_X-CHBNC and MnO_X-KLBNC adsorbents were washed with deionized water, dried at 70 ℃ for 2 hours, and reused for the successive cycle [26].

RESULTS AND DISCUSSION

Adsorbent characterization

Figure 1 presents the XRD patterns of CHB, KLB, MnO_X-CHBNC, and MnO_X-KLBNC, which consist of natural cellulose, lignin, and non-crystalline hemicelluloses. The diffraction peaks observed at 2θ = 16.1, and 22.4 are due to natural cellulose [27]. Reports confirm that the large d-spacing in the XRD peaks of biochar is due to the presence of unconverted cellulose and the existence of -OH, C=O-C, and C-O groups [21]. In general, the XRD patterns and the SEM images (Figure 2) have revealed that both pristine and MnOx-nanocomposites of CH and KL biochars are amorphous.

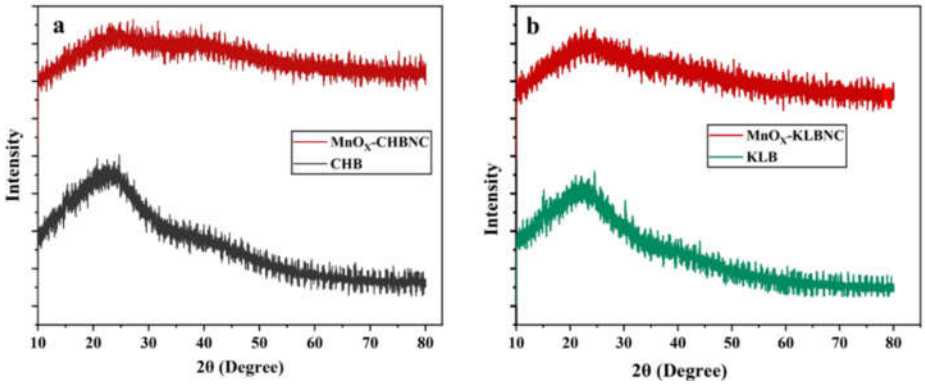

Figure 1. XRD patterns of (a) CHB and MnO_X-CHBNC; (b) KLB and MnO_X-KLBNC.

Figure 2 shows the SEM images taken to observe the textural properties and morphological changes in the MnO_X nanocomposite biochar and the pristine biochars of CH and KL. These images confirmed the amorphous and heterogeneous structures of the biochars. Pores were observed in all biochars, which were formed due to the escape of volatile substances and the

formation of channel structure during pyrolysis [28]. Figures 2b and 2d show that the formation of a larger pore structure is more prominent in MnO_X-CHBNC and MnO_X-KLBNC. This is expected because activation is known to increase porosities and enlarge the diameter of smaller pores created during pyrolysis [29].

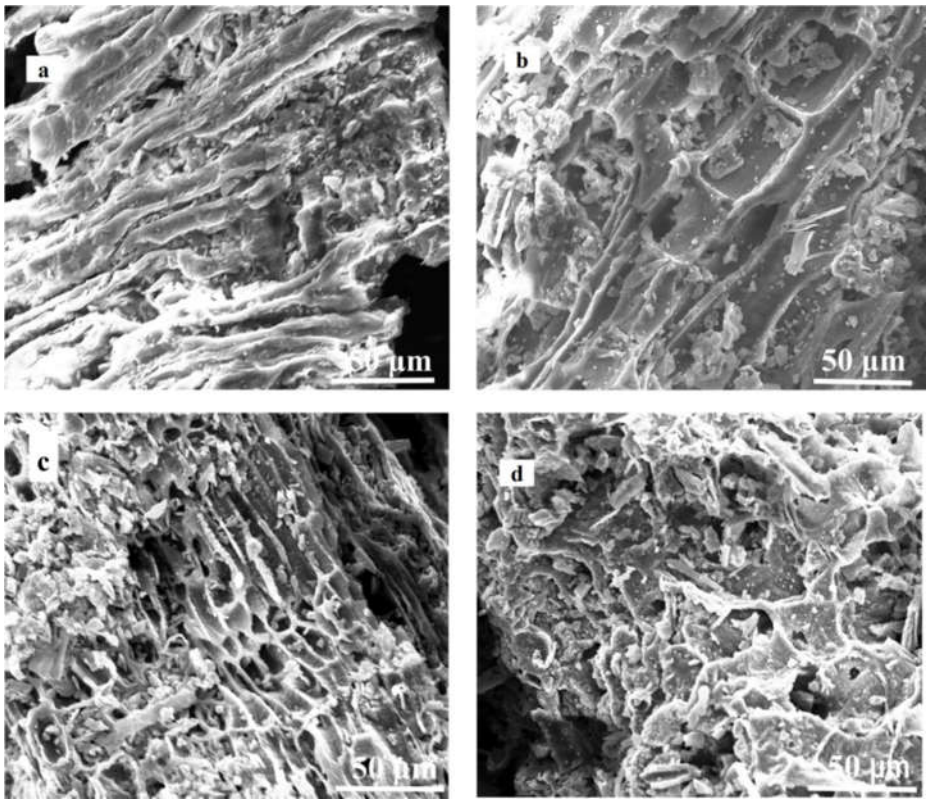

Figure 2. SEM images of pristine and activated CH and KL biochars; (a) CHB; (b) MnO_X-CHBNC; (c) KLB; (d) MnO_X-KLBNC.

FTIR spectroscopy was used to identify the presence of various surface functional groups, such as amino, carbonyl, carboxyl, and others [30]. Figures 3a and 3b show the results of FTIR analyses conducted on CHB, MnO_X-CHBNC, KLB, and MnO_X-KLBNC. The findings indicate the existence of functional groups such as O-H (3417-3426 cm^{-1}), C-H (2853-2920 cm^{-1}), C=C (1611-1622 cm^{-1}), and C-O (1411-1466 cm^{-1}) [31-33]. Peaks at 437 and 525 cm^{-1} for MnO_x-CHBNC, as well as strong peaks at 464, 545, and 781 cm^{-1} for MnO_x-KLBNC, characterize the bonds in R-MnOx, indicating the presence of MnO_X in the activated biochar [34]. These groups play a crucial role in Cr(VI) adsorption through electrostatic interaction [35]. The broad O-H bands observed in MnO_X-CHB and MnO_X-KLBNC are attributed to the additional source of the -OH group from moisture [36].

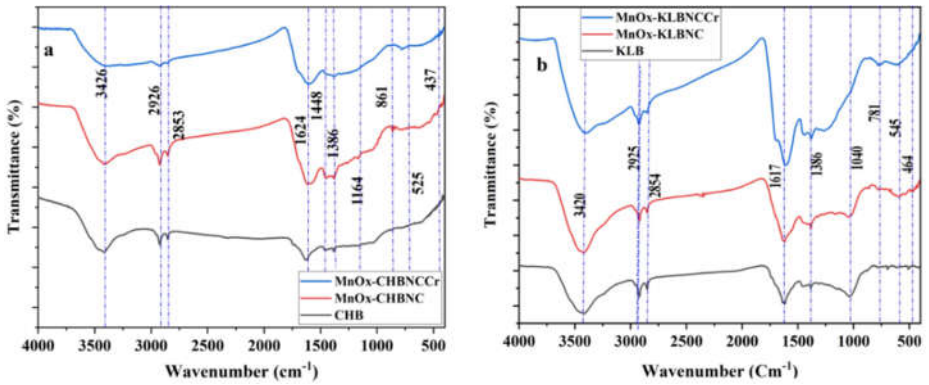

Figure 3. FTIR spectra of (a) CHB and MnO_X-CHBNC; (b) KLB and MnO_X-KLBNC.

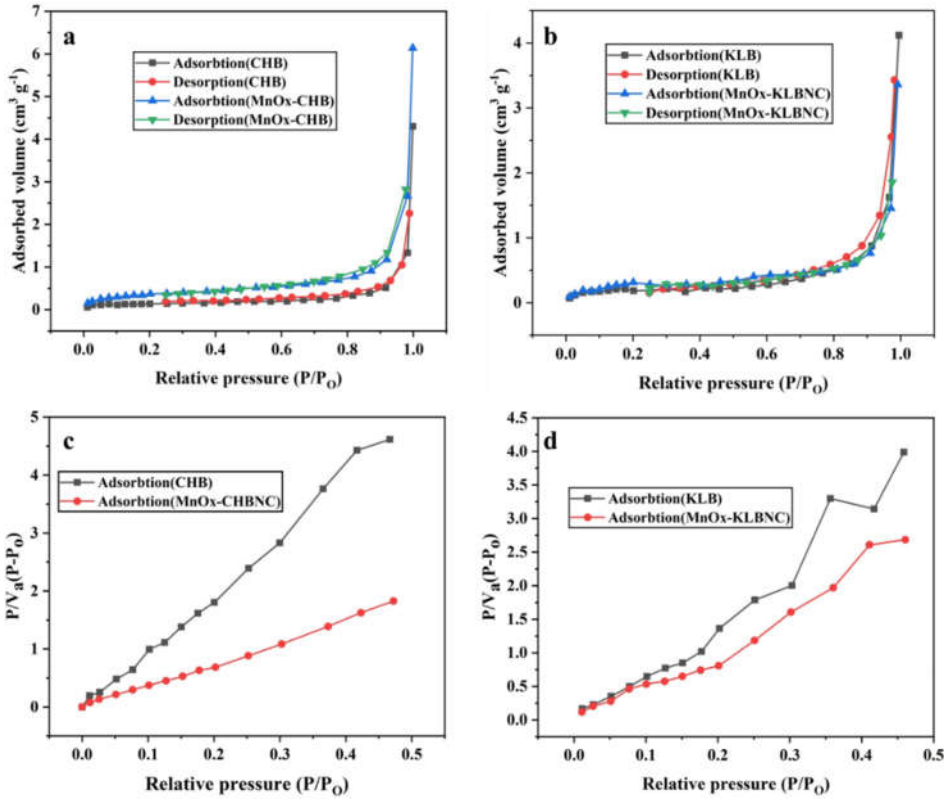

Figure 4. Adsorption-desorption isotherm of nitrogen on (a) CHB and MnO_X-CHBNC; (b) KLB and MnO_X-KLBNC; BET analysis plot of (c) CHB and MnO_X-CHBNC; (d) KLB and MnO_X-KLBNC.

Figures 4a - d display the adsorption-desorption isotherm and BET analysis plots for the CHB, MnO_X-CHBNC, KLB, and MnO_X-KLBNC. Based on the results of BET analysis, the specific surface area, pore volume and pore size for CHB were 0.519 m^2 g^{-1}, 0.004 cm^3 g^{-1}, and 32.804 nm, respectively. For MnO_X-CHBNC, the values were 1.289 m^2 g^{-1}, 0.006 cm^3 g^{-1}, and 21.218 nm, KLB showed values of 0.826 m^2 g^{-1}, 0.005 cm^3 g^{-1}, and 27.626 nm, while MnO_X-KLBNC had values of 1.03 m^2 g^{-1}, 0.006 cm^3 g^{-1} and 19.511nm. The results indicated that MnO_X-CHBNC and MnO_X-KLBNC had higher specific areas, total pore volumes, and smaller pore sizes than their pristine biochars. Additionally, according to IUPAC, the adsorption-desorption isotherm and BET analysis showed that the adsorbents exhibited mesoporous structures [37].

Batch adsorption studies

Preliminary tests were conducted to select an adsorbent for removing Cr(VI) from an aqueous solution. The results showed that CH, KL, MnO_X-CHBNC, and MnO_X-KLBNC exhibited varying efficiencies in removing Cr(VI). The Cr(VI) removal efficiencies of CH and KL biochars were significantly lower than those of their MnOx-nanocomposites: MnO_X-CHBNC, and MnO_X-KLBNC, which removed 74.98% and 84.78% of Cr(VI) from the aqueous solution respectively. Therefore, MnO_X-CHBNC and MnO_X-KLBNC were chosen for removing Cr(VI) from water. The parameters that can affect the Cr(VI) adsorption efficiency of MnO_X-CHBNC and MnO_X-KLBNC were investigated at a constant temperature of 25 °C.

pH point of zero charge

The pH point of zero charge (pH_{PZC}) of an adsorbent depends on the chemical and electronic properties of the functional groups on its surface. To determine the pH_{PZC}, the salt addition technique described by Elisee and coworkers was used. Initially, a 40 mL solution of 0.1 M $NaNO_3$ was added to a series of 50 mL centrifuge tubes. The pH was then adjusted to varied values ranging from 2 – 11 at unit intervals using 0.1 M solutions of HNO_3 and NaOH resulting in pH values denoted as pH_i.

Subsequently, 0.2 g of each adsorbent was added to the tubes, and the mixtures were shaken continuously at 200 rpm for 24 h. Afterwards, the pH of the supernatant in each tube was measured, and these values were recorded as pH_f. The pH_{PZC} was determined by identifying the x-intercept of the ΔpH (pH_f - pH_i) plotted against pH_i. The results of the pH_{PZC} determination are shown in Figure 5a, with pH_{PZC} values estimated at pH 7.82 for MnO_X-CHBNC and 8.43 for MnO_X-CHBNC. Therefore, to ensure that the positively charged surfaces facilitate adsorption through electrostatic attraction between the adsorbents and the anions, pH values should be maintained below these values.

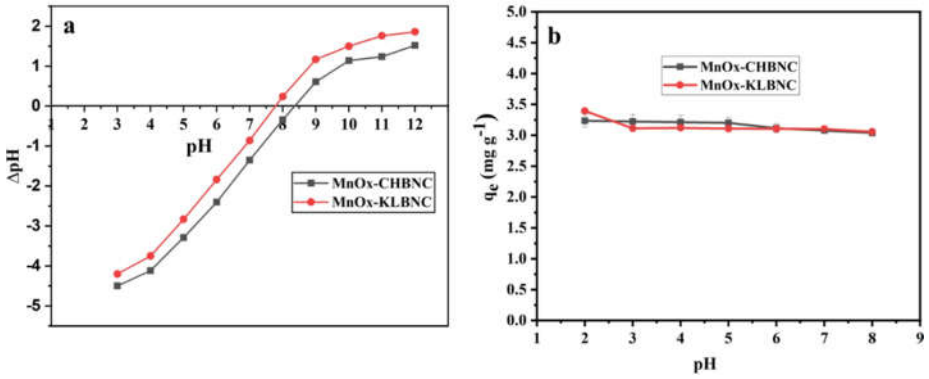

Figure 5. (a) The pH_{PZC} of MnO_X-CHBNC and MnO_X-KLBNC; (b) The effect of pH on q_e.

The effect of pH

In general, the pH of the solution affects the adsorption processes, results from the functional groups of the adsorbent, and changes in the surface charge of the adsorbent [38]. The effect of pH on Cr(VI) adsorption was evaluated in the pH range of 2 - 8 (Figure 5b). The pH of the solutions was adjusted using 0.10 M HNO_3 and 0.10 M NaOH solutions [39]. Figure 5b illustrates the effect of initial pH on the Cr(VI) adsorption capacity of the MnO_X-CHBNC and MnO_X-KLBNC. In this study the initial Cr(VI) concentration was 20 mg L^{-1}; the adsorbent dose was 0.1 g for both MnO_X-CHBNC and MnO_X-KLBNC; the temperature was 25 °C, and the contact time was 60 min. The results showed that the adsorption capacity is sensitive to pH changes and relatively the highest values were observed when the pH of the Cr(VI) solution was 2. Thus, pH 2 was chosen as the optimum value in further studies.

The effect of adsorbent dose

The effect of dose on Cr(VI) adsorption capacities was evaluated using 0.05, 0.1, 0.15, 0.2, 0.25, 0.3, 0.4, and 0.5 grams of adsorbents [40].

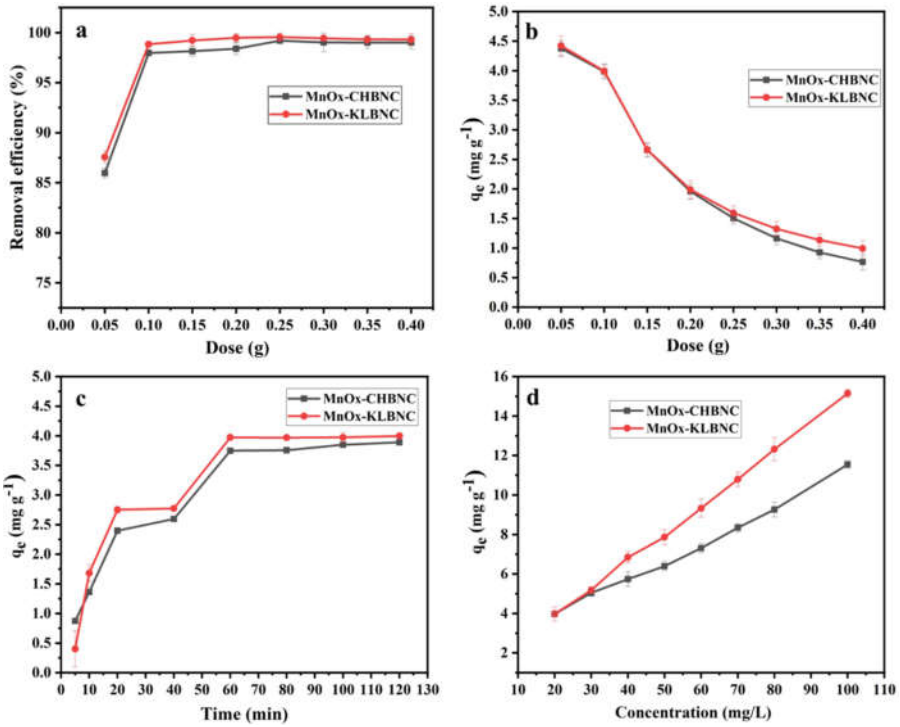

Figure 6. (a) The effect of adsorbent dose on removal efficiency; (b) the effect of adsorbent dose on adsorption capacity; (c) the effect of time; (d) the effect of the initial concentration on the adsorption capacity of MnO_X-CHBNC and MnO_X-KLBNC to remove Cr(VI) from water.

Figures 6a and 6b show that at the various dosages of MnO_X-CHBNC and MnO_X-KLBNC, there are significant variations in the removal efficiencies of Cr(VI) and the adsorption capacities. It can be observed that when the dosage of MnO_X-CHBNC and MnO_X-KLBNC increased from 0.05 g to 0.10 g, the removal efficiency of Cr(VI) significantly increased and remained slightly constant above 0.10 g. The increase in removal efficiency with a higher adsorbent dose is due to the availability of more binding sites for Cr(VI) adsorption, reaching a saturation point at a certain dosage. Therefore, for both MnO_X-KLBNC and MnO_X-CHBNC, 0.10 g has been chosen for subsequent studies.The adsorbent dose negatively influenced the adsorption capacity (Figure 6b). The q_e value decreased rapidly when the MnO_X-CHBNC and MnO_X-KLBNC doses changed from 0.05 to 0.5 g L^{-1}. Subsequently, the slope of the curve of adsorption capacity decreased because when the amount of the adsorbent is low, the active adsorption sites can rapidly combine with adsorbates and approach saturation. When the amount of adsorbent exceeds a certain value, increasing adsorption sites fail to come in contact with adsorbate molecules [41]. Additionally, as the amounts of adsorbents increase, it is easier for them to aggregate, thereby reducing the specific surface area of the adsorbents [42].

Effect of contact time

Contact time is one of the factors that affect adsorption capacity. Reports indicate that adsorption capacity increases with longer contact time [35]. Figure 6a shows that Cr(VI) adsorption on the prepared materials was rapid during the initial stages of adsorption. It then gradually increased after 20 min and remained relatively constant after 60 min for both MnO_X-CHBNC and MnO_X-KLBNC. The results indicate that adsorption takes place rapidly at the beginning due to the availability of sufficient adsorption surface sites, but the rate slows down over time until equilibrium is reached. The remaining adsorption sites face obstacles to continuous adsorption because of repulsive forces between solute molecules adsorbed on the solid and the bulk phase [43].

The effect of initial concentration

The effect of initial concentration and isotherm model was studied using initial concentrations of 10-100 mg L^{-1}. The other parameters were kept constant (pH 2, adsorbent dose 0.1 g, and contact time 60 min). Figure 6d describes how the adsorption efficiency depends on the initial Cr(VI) concentration. The results showed that the Cr(VI) adsorption capacity of the adsorbents increased with increasing the initial concentration of Cr(VI). The adsorption capacity of MnO_X-CHBNC changed from 3.97 to 11.55 mg g^{-1}, while MnO_X-CHBNC changed from 3.97 to 15.15 mg g^{-1}. Generally, the adsorption of molecules seems to occur more readily at higher initial concentrations due to the presence of a higher driving force required for the mass transfer of Cr(VI) ions. In addition, it can be noticed that a longer equilibrium time was required for solutions with high initial concentrations. This is because, at the final stage of adsorption, most of the sorbate molecules diffuse into the porous structure of the adsorbent as the adsorbent surface is saturated [44].

Conversely, the removal efficiency decreases with increased Cr(VI) concentration. At the optimum adsorption conditions, MnO_X-CHBNC and MnO_X-KLBNC removed about 99.63% and 99.84%, respectively. When the concentration of Cr(VI) is higher than 20 mg L^{-1}, the removal efficiency significantly decreased for MnO_X-CHBNC and MnO_X-KLBNC. Out of the two adsorbents, MnO_X-KLBNC demonstrated superior efficiency in removing Cr(VI) compared to MnO_X-CHBNC, particularly at relatively higher initial concentrations. At lower concentrations of Cr(VI), removal efficiency is higher due to the increased mobility of ions in dilute solutions. Meanwhile, when the initial concentration was increased with a constant adsorbent mass, the reduction of adsorption efficiency can be caused by the shortage of active sites for binding Cr(VI) [8].

Adsorption isotherm and kinetics model

The adsorption equilibrium was studied by fitting the experimental data to the linear equations of Langmuir (Equation 3) and Freundlich (Equation 4) isotherm models [45].

Langmuir isotherm model: $\frac{C_e}{q_e} = \frac{1}{K_L q_m} + \frac{C_e}{q_m}$ (3)

Freundlich isotherm model: $logq_e = logK_F + \frac{1}{n} log\ C_e$ (4)

where q_e (mg g^{-1}) is the amount of adsorbate adsorbed; C_e (mg L^{-1}) is the adsorbate concentration in the solution at equilibrium; K_L is the Langmuir adsorption constant, and q_m (mg g^{-1}) is the maximum adsorption capacity for monolayer formation on the adsorbent [46]. The value K_F is the adsorption or distribution coefficient and represents the number of ions adsorbed onto the surface of the adsorbent particle. The value of 1/n indicates surface heterogeneity, which becomes more heterogeneous as its value gets closer to zero [47]. A fundamental characteristic of the Langmuir isotherm is to predict the affinity between adsorbate and sorbent using a dimensionless constant, known as the separation factor R_L, which can be described as Equation 5.

$$R_L = \frac{1}{1+K_L C_o} \quad (5)$$

where C_o (mgL^{-1}) is the adsorbate initial concentration. The value of R_L stands between 0 and 1 for favorable adsorption, while $R_L > 1$ represents unfavorable adsorption, $R_L = 1$ represents linear adsorption, and $R_L = 0$ for irreversible adsorption processes [47].

Adsorption isotherms relate to the adsorbate concentration and adsorption capacity at a specific adsorbent dose and temperature [9]. Analysis of these isotherms also provides a better understanding of the adsorption mechanisms, which depend on factors such as surface polarity, surface area, and porosity. Linear forms of the Langmuir and Freundlich isotherm models were used to quantify the equilibrium adsorption data [48]. The Langmuir isotherm (Equation 3) describes monolayer adsorption on a homogeneous surface with uniform active sites.

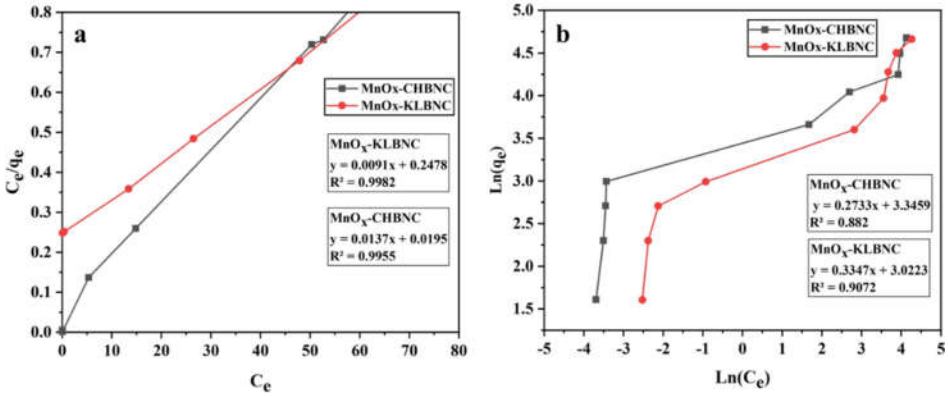

Figure 7. (a) Langmuir isotherm for MnO_X-CHBNC and MnO_X-KLBNC; (b) Freundlich isotherm MnO_X-CHBNC and MnO_X-KLBNC.

The Langmuir and Freundlich isotherm parameters and their related correlation coefficients are shown in Figure 7 and Table 1. A higher correlation coefficient (R^2) indicates the greater applicability of the Langmuir model (R^2 = 0.996) for MnO_X-CHBNC) and (R^2 = 0.99 for MnO_X-

KLBNC), illustrating the monolayer adsorption on specific site of a homogeneous surface of the adsorbent [49]. The Langmuir isotherm predicts that adsorption energy is uniform on the adsorbent surface and that no interaction exists between the adsorbed molecules [50]. The low separation factor values (R_L = 0.011 - 0.258 for MnO_X-CHBNC and R_L= 0.044 - 0.520 for MnO_X-KLBNC) imply a favorable physical adsorption process. The Freundlich isotherm demonstrates multilayered adsorption for heterogeneous surfaces or surface-supporting sites of different affinities [33]. The calculated values of n falling in the range of 1-10 indicate favorable sorption. Furthermore, the Langmuir isotherm model has a higher regression coefficient R^2 than the Freundlich model (Figures 7a and b), showing that the Langmuir model provides a better description. These results suggest monolayer adsorption of Cr(VI) on the surface of both adsorbents.

Table 1. Langmuir and Freundlich isotherm constants for adsorption of Cr(VI).

Isotherm model	MnO_X-CHBNC	MnO_X-KLBNC
Langmuir	y = 0.0137x + 0.0195	y = 0.0091x + 0.2478
q_m	72.993	109.890
K_L	0.144	0.037
R_L	0.011 - 0.258	0.044 - 0.520
R^2	0.996	0.998
Freundlich	y = 0.2733x + 3.3459	y = 0.3134x + 2.9906
N	3.659	3.191
K_F	28.386	19.898
R^2	0.882	0.9268

Kinetic studies were conducted using a solution with initial concentrations of 20, 100, and 300 mg L^{-1} at pH 2, using 0.1 g of MnO_X-CHBNC and MnO_X-KLBNC separately. The effect of time was studied from 5 - 240 min. After shaking at 200 rpm for the specified time, the solutions were filtered, and the) concentrations of Cr(VI) were determined. The amount of Cr(VI) adsorbed onto MnO_X-CHBNC and MnO_X-KBNC at time t (q_t) was calculated using Equation 6.

$$q_t = \frac{(C_o - C_t)V}{m} \quad (6)$$

where C_o is the initial concentration (mg L^{-1}), C_t is the concentration at time t (mg L^{-1}), V is the volume (L), and m is the mass of the adsorbent (g).

The following equations were used in the adsorption kinetics models. Equation 7 describes the pseudo-first-order adsorption kinetics:

$$ln(q_e - q_t) = ln(q_e) - K_1 t \quad (7)$$

where q_e and q_t are the amounts of Cr(VI) adsorbed (mg g^{-1}) at equilibrium and time t (min), respectively, K_1 is the rate constant for the pseudo-first-order kinetics model.
Equation 8 represents the pseudo-second-order kinetics

$$\frac{t}{q_t} = \frac{1}{K_2 {q_e}^2} + \frac{1}{q_e} \quad (8)$$

K_2 is the rate constant for the pseudo-second-order kinetic adsorption model. The adsorption parameters, including R^2 and other constants, were calculated for both models and are listed in Table 2. In this study, the pseudo-first-order model was determined to better represent the adsorption mechanism. This indicates that the mass transfer from the bulk solution to the adsorption sites on the adsorbent surface is the rate-limiting step in the adsorption process. The rate of adsorption is influenced by the concentration disparity between the adsorbate in the

solution and the available sites on the adsorbent. This model is more closely related to physisorption rather than chemisorption [8].

Table 2. Constants of pseudo-first and second-order adsorption kinetic models.

Adsorbent	Kinetic Model	Initial Cr(VI) Concentration		
		20 $mg.L^{-1}$	100 $mg.L^{-1}$	300 $mg.L^{-1}$
MnO_X-CHBNC	experimental	3.985	22.31	73.52
	Pseudo-first order			
	q_e	1.128	21.93	74.612
	K_1	5.10×10^{-2}	7.40×10^{-3}	5.90×10^{-3}
	R^2	0.755	0.970	0.966
	Pseudo-second order			
	q_e	4.364	32.787	99.011
	K_2	3.90×10^{-1}	1.702×10^{-4}	4.735×10^{-5}
	R^2	0.985	0.4994	0.5719
MnO_X-KLBC	$q_{experimental}$	3.993	29.346	97.660
	Pseudo-first order			
	q_e	3.755	25.644	83.856
	K_1	2.51×10^{-2}	1.65×10^{-2}	5.40×10^{-3}
	R^2	0.463	0.970	0.989
	Pseudo-second order			
	q_e	3.987	32.787	66.667
	K_2	6.613×10^{-1}	80586×10^{-3}	3.891×10^{-4}
	R^2	0.999	0.954	0.841

Comparison with other similar studies

The maximum adsorption capacities and Cr(VI) removal efficiency of certain reported adsorbents are described in Table 3. The adsorption capacities achieved by the MnO_X-CHBNC and MnO_X-KLBNC prepared in this study were higher than some adsorbents and lower than others. However, upon comparison, it is clear that the amount of adsorbents used in this study is smaller than that used in the previous reports listed in Table 3. Therefore, the MnO_X-CHBNC and MnO_X-KLBNC are viable alternative adsorbents for removing Cr(VI) from an aqueous solution. Furthermore, producing biochar-nanocomposites from CH and KL provides an effective method for removing potential pollutants and creating value-added treatment products. CH and KL are ideal, and cost-effective biomass sources for biochar production, making this method suitable for resource recovery and environmental protection.

Table 3. Comparison of the Cr(VI) removal efficiency of some adsorbents from aqueous solution.

Adsorbent	C_o ($mg.L^{-1}$)	Volume (mL)	m (g)	q_m ($mg.g^{-1}$)	R efficient (%)	Refer.
ZnO-bagasse biochar	50.00	50.00	0.10	102.66	92	[2]
FeS-wheat straw biochar	50.00	42.00	0.72	150.00	95	[22]
Magnetic woodchip biochar	10.00	50.00	0.50	80.96	95	[25]
Activated shaddock biochar	20.00	25.00	0.05	9.95	99.2	[44]
Modified corn stalk biochar	50.00	50.00	0.10	25.68	ND	[10]
Clay-$MnFe_2O_4$ composite	10.00	25.00	0.10	178.60	98.65	[37]
MnO_X-CHBNC	20.00	20.00	0.10	72.99	99.63	This study
MnO_X-KLBNC	20.00	20.00	0.10	109.84	99.89	This study

Reusability of the adsorbents

The advantage of the proposed biochar-nanocomposite adsorbents is their easy separation from soluble waste and reusability. 2 g of MnO_X-CHBNC and MnO_X-KLBNC in a 250 mL solution of Cr(VI) with a concentration of 20 mg L^{-1} were used for Cr(VI) removal under optimum parameters. The relative adsorption capacities were calculated concerning the MnO_X-CHBNC and MnO_X-KLBNC without recycling. The study showed that during the recycling of the sorbent, after the first use, the relative adsorption capacity of MnO_X-CHBNC was 99.37% and 99.83% for MnO_X-KLBNC. After six cycles, the values slightly decreased to 95.12% for MnO_X-CHBNC and 98.12% for MnO_X-KLBNC. The results revealed that by the sixth cycle, the Cr(VI) adsorption capacities of both adsorbents are promising. Therefore, due to their low cost, ease of preparation, and better reusability cycles, MnO_X-CHBNC and MnO_X-KLBNC could be used for Cr(VI) removal.

CONCLUSION

Pristine biochar of CH, synthesized by pyrolysis of biomass at 300 °C, removes 74.98% of Cr(VI), while KL removes 84.78% from 20 mgL^{-1} aqueous solutions. MnO_X-CHBNC and MnO_X-KLBNC synthesized by pretreating every 25 g of dried biomass with 12.5 mmol of $KMnO_4$ and pyrolyzed at 300 °C for 60 min have an efficiency of 99.63% and 99.84% in removing Cr(VI) from 20 mg L^{-1} aqueous solution using 0.1 g of MnO_X-CHBNC and MnO_X-KLBNC, respectively, in 120 min. Maximum removal efficiencies and adsorption capacities were investigated by optimizing parameters such as adsorbent dose, pH, contact time, and initial concentration of the solution.

Equilibrium data fit very well in the Langmuir isotherm equation, confirming the monolayer adsorption mechanism of Cr(VI) onto the adsorbents is more dominant. Linear plots were drawn for Langmuir and Freundlich isotherm in both adsorbents. In the Langmuir isotherm, the value of R_L lies between zero and one, indicating favorable adsorption. Cr(VI) adsorption was found to fit a pseudo-first-order model, in which adsorption depends on adsorption site availability. The results confirm that the proposed method is effective for CH and KL recycling and low-cost carbon material preparation. This laboratory scale data should be tested using real water samples from industrial effluent to establish a baseline for designing treatment plants to clean Cr(VI)-containing effluents.

ACKNOWLEDGEMENTS

We are grateful to the College of Natural Sciences at Jimma University for providing financial support through the grand research project (CNS-Chem-11-2020/21-SP3). Jemere Kochito also acknowledges Mizan-Tepi University for sponsoring his PhD studies.

REFERENCES

1. Liang, Y.; Yi, X.; Dang, Z.; Wang, Q.; Luo, H.; Tang, J. Heavy metal contamination and health risk assessment in the vicinity of a tailing pond in Guangdong, China. *Int. J. Environ. Res. Public Health*. **2017**, 14, 1557.
2. Gan, C.; Liu, Y.; Tan, X.; Wang, S.; Zeng, G.; Zheng, B.; Li, T.; Jiang, Z.; Liu, W. effect of porous zinc-biochar nanocomposites on Cr (VI) adsorption from aqueous solution. *RSC Adv.* **2015**, *5*, 35107–35115.
3. Yifru, A.; Mekonnen, N.; Mehretie, S.; Admassie, S. Polypyrrole–polyaniline-water hyacinth leaf protein concentrate composite for the removal of Cr(VI) from aqueous solution: kinetics, isotherm and thermodynamic studies. *Bull. Chem. Soc. Ethiop*. **2022**, 36 (3), 571–584.
4. Marghaki, N.S.; Jonoush, Z. A.; Rezaee, A. Improving the performance of Cr (VI) Removal by electrochemical process using microbial cellulose/magnetic nanoparticles electrode. *J.*

Clean. Prod. **2020**, 277, 123195.
5. Yao, Z.; Du, S.; Zhang, Y.; Zhu, B.; Zhu, L.; John, A.E. Positively charged membrane for removing low concentration Cr(VI) in ultrafiltration process. *J. Water Process Eng.* **2015**, 8, 99–107.
6. Dharnaik, A.S.; Ghosh, P.K. Hexavalent chromium [Cr(VI)] removal by the electrochemical ion-exchange process. *Environ. Technol.* **2014**, 35, 2272–2279.
7. Verma, B.; Balomajumder, C. Hexavalent Chromium reduction from real electroplating wastewater by chemical precipitation. *Bull. Chem. Soc. Ethiop.* **2020**, 34, 67–74.
8. Singh, S.; Anil, A.G.; Khasnabis, S.; Kumar, V.; Nath, B.; Adiga, V.; Kumar Naik, T.S.S.; Subramanian, S.; Kumar, V.; Singh, J.; Ramamurthy, P.C. Sustainable removal of Cr(VI) using graphene oxide-zinc oxide nanohybrid: adsorption kinetics, isotherms and thermodynamics. *Environ. Res.* **2022**, 203, 111891.
9. Xu, G.; Zhu, Y.; Xiinjun, W.; Wang, S.; Cheng, T.; Ping, R.; Cao, J.; Lv, K. Novel chitosan and laponite based nanocomposite for fast removal of Cd(II), methylene blue and congo red from aqueous solution. *e-Polymers* **2019**, 19, 244–256.
10. An, Q.; Li, X.-Q.; Nan, H.-Y.; Yu, Y.; Jiang, J.-N. The Potential adsorption mechanism of the biochars with different modification processes to Cr (VI). *Environ. Sci. Pollut. Res.* **2018**, 25, 31346–31357.
11. Tong, X.-J.; Li, J.-Y.; Yuan, J.-H.; Xu, R.-K. Adsorption of Cu(II) by biochars generated from three crop straws. *Chem. Eng. J.* **2011**, 172, 828–834.
12. Moazzam, A.; Jamil, N.; Nadeem, F.; Qadir, A.; Ahsan, N.; Zameer, M. Reactive dye removal by a novel biochar/ MgO nanocomposite. *J. Chem. Soc. Pakistan* **2017**, 39, 26–34.
13. Ray, P.Z.; Shipley, H.J. Inorganic nano-adsorbents for the removal of heavy metals and arsenic: a review. *RSC Adv.* **2015**, 5, 29885–29907.
14. Lu, F.; Astruc, D. Nanomaterials for removal of toxic elements from water. *Coord. Chem. Rev.* **2018**, 356, 147–164.
15. Tan, X.f.; Liu, Y.-g.; Gu, Y.-l.; Xu, Y.; Zeng, G.-m.; Hu, X.-j.; Liu, S.-b.; Wang, X.; Liu, S.-m.; Li, J. Biochar-based nano-composites for the decontamination of wastewater: A review. *Bioresour. Technol.* **2016**, 212, 318–333.
16. Godwin, P.M.; Pan, Y.; Xiao, H.; Afzal, M.T. Progress in preparation and application of modified biochar for improving heavy metal ion removal from wastewater. *J. Bioresour. Bioprod.* **2019**, 4, 31–42.
17. Amamo, A. A. Coffee production and marketing in Ethiopia. *Eur. J. Bus. Manag.* **2014**, 6, 109–122.
18. Kebede, T.; Berhe, D.T.; Zergaw, Y. Combustion Characteristics of briquette fuel produced from biomass residues and binding materials. *J. Energy* **2022**, 2022,4222205.
19. Mubarak, N.M.; Kundu, A.; Sahu, J.N.; Abdullah, E.C.; Jayakumar, N.S. Synthesis of palm oil empty fruit bunch magnetic pyrolytic char impregnating with $FeCl_3$ by microwave heating technique. *Biomass Bioenergy* **2013**, 61, 265–275.
20. Zheng, Y.; Zimmerman, A.R.; Gao, B. Comparative Investigation of characteristics and phosphate removal by engineered biochars with different loadings of magnesium, aluminum, or iron. *Sci. Total Environ.* **2020**, 747, 141277.
21. Giraldo, S.; Robles, I.; God, L. A.; Acelas, N. Experimental and theoretical insights on methylene blue removal from wastewater using an adsorbent obtained from the residues of the orange industry. *Molecules* **2021**, 26, 4555.
22. Zewdu, F.; Amare, M. Determination of the level of hexavalent, trivalent, and total chromium in the discharged effluent of Bahir Dar tannery using ICP-OES and UV-Visible spectrometry. *Cogent Chem.* **2018**, 4, 1534566.
23. Liu, H.; Tang, J.; Huang, Y.; Gai, L.; Zeng, E. Y.; Liber, K.; Gong, Y. Removal of hexavalent chromium from aqueous solutions by a novel biochar supported nanoscale iron sulfide composite. *Chem. Eng. J.* **2017**, 322, 516–524.

24. Haider, Z.; Gao, M.; Qiu, W.; Song, Z. Mechanisms for cadmium adsorption by magnetic biochar composites in an aqueous solution. *Chemosphere* **2020**, 246, 125701.
25. Ma, Y.; Liu, W.; Zhang, N.; Li, Y.; Jiang, H.; Sheng, G. Polyethylenimine modified biochar adsorbent for hexavalent chromium removal from the aqueous solution. *Bioresour. Technol.* **2014**, 169, 403–408.
26. Pan, J.; Jiang, J.; Xu, R. Adsorption of Cr(III) from Acidic solutions by crop straw derived biochars. *J. Environ. Sci.* **2013**, 25, 1957–1965.
27. Ali, S.; Zhu, J.; Muhammad, N.; Sheng, T. Effect of synthesis methods on magnetic kans grass biochar for enhanced As(III, V) adsorption from aqueous solutions. *Biomass Bioenergy* **2014**, 71, 299-310.
28. Goswami, R.; Shim, J.; Deka, S.; Kumari, D.; Kataki, R. Characterization of cadmium removal from aqueous solution by biochar produced from *Ipomoea fistulosa* at different pyrolytic temperatures. *Ecol. Eng.* **2016**, 97, 444–451.
29. Enaime, G.; Baçaoui, A.; Yaacoubi, A.; Lübken, M. Biochar for wastewater treatment-conversion technologies and applications. *Appl. Sci.* **2020**, 10, 3492.
30. Zhao, F.; Shan, R.; Gu, J.; Zhang, Y.; Yuan, H.; Chen, Y. Magnetically recyclable loofah biochar by $KMnO_4$ modification for adsorption of Cu(II) from aqueous solutions. *ACS Omega* **2022**, 7, 8844–8853.
31. Zheng, Y.; Wang, J.; Li, D.; Liu, C.; Lu, Y.; Lin, X. Insight into the KOH /$KMnO_4$ activation mechanism of oxygen-enriched hierarchical porous biochar derived from biomass waste by in-situ pyrolysis for methylene blue enhanced adsorption. *J. Anal. Appl. Pyrolysis* **2021**, 158, 105269.
32. Abd-Elhamid, A.I.; Emran, M.; El-Sadek, M.H.; El-Shanshory, A.A.; Soliman, H.M.A.; Akl, M.A.; Rashad, M. Enhanced removal of cationic dye by eco-friendly activated biochar derived from rice straw. *Appl. Water Sci.* **2020**, 10, 45.
33. Paredes-Laverde, M.; Salamanca, M.; Diaz-Corrales, J.D.; Fl, E.; Silva-Agredo, J.; Torres-Palma, R.A. Understanding the removal of an anionic dye in textile wastewaters by adsorption on $ZnCl_2$ Activated carbons from rice and coffee husk wastes: a combined experimental and theoretical study. *J. Environ. Chem. Eng.* **2021**, 9, 105685.
34. Julien, C.M. Local structure of lithiated manganese oxides. *Solid State Ionics* **2006**, 177, 11–19.
35. Qin, Q.; Wang, Q.; Fu, D.; Ma, J. An efficient approach for Pb(II) and Cd(II) Removal using manganese dioxide formed in situ. *Chem. Eng. J.* **2011**, 172, 68–74.
36. Kumari, S.; Hari, S.; Annamareddy, K. Treatment of garage wastewater using activated carbon made from Khat (*Catha edulis*) and Neem (*Azadirachta indica*) leaves. *Environ. Dev. Sustain.* **2020**, 22, 2967–2978.
37. Ahmadi, A.; Foroutan, R.; Esmaeili, H. The role of bentonite clay and bentonite clay @ $MnFe_2O_4$ Composite and their physico-chemical properties on the removal of Cr(III) and Cr(VI) from aqueous media. *Environ. Sci. Pollut. Res.* **2020**, 27, 14044–14057.
38. Ma, J.; Yu, F.; Zhou, L.; Jin, L.; Yang, M.; Luan, J.; Tang, Y.; Fan, H.; Yuan, Z.; Chen, J. Enhanced adsorptive removal of methyl orange and methylene blue from aqueous solution by alkali-activated multiwalled carbon nanotubes. *ACS Appl. Mater. Interfaces* **2012**, 4, 5749–5760.
39. Maniyam, M.N.; Hari, M. Optimization of culture conditions for improved green biodecolorization of methylene blue by *Rhodococcus pyridinivorans* strain UCC 0003. *BioTechnologia (Pozn).* **2021**, 102, 125–140.
40. Zeghioud, H.; Fryda, L.; Mathieu, A.; Visser, R.; Kane, A. Potential of flax shives and beech wood-derived biochar in methylene blue and carbamazepine removal from aqueous solutions. *Materials* **2022**, 15, 2824.
41. Song, X.; Li, L.; Geng, Z.; Zhou, L.; Ji, L. Effective and Selective adsorption of As(III) via imprinted magnetic Fe_3O_4/HTCC composite nanoparticles. *J. Environ. Chem. Eng.* **2017**, 5,

16–25.
42. Fakhri, A. Adsorption characteristics of graphene oxide as a solid adsorbent for aniline removal from aqueous solutions: Kinetics, thermodynamics and mechanism studies. *J. Saudi Chem. Soc.* **2017,** 21, S52-S57.
43. Sukhbaatar, B.; Yoo, B.; Lim, J. Metal-Free high-adsorption-capacity adsorbent derived from spent coffee grounds for methylene blue. *Royal Soc. Chem.* **2021**, 11, 5118–5127.
44. Tao, X.; Wu, Y.; Cha, L. Shaddock peels-based activated carbon as cost-saving adsorbents for efficient removal of Cr(VI) and methyl orange. *Environ. Sci. Pollut. Res.* **2019**, 26, 19828–19842.
45. De Caprariis, B.; De Filippis, P.; Petrucci, E.; Scarsella, M. Activated biochars used as adsorbents for dyes removal. *Chem. Eng. Trans.* **2018**, 6, 103–108.
46. Santhosh, C.; Daneshvar, E.; Tripathi, K. M.; Baltrėnas, P.; Kim, T. Y.; Baltrėnaitė, E.; Bhatnagar, A. Synthesis and characterization of magnetic biochar adsorbents for the removal of Cr(VI) and acid orange 7 dye from aqueous solution. *Environ. Sci. Pollut. Res.* **2020**, 27, 32874–32887.
47. Lisandra de Castro, A.; Susana, Y.-V.; Yolanda, P.-R.; José, R. Efficient separation of heavy metals by magnetic nanostructured beads. *Inorganics* **2020**, 8, 40.
48. Subratti, A.; Ladeira, J.; Lalgee, L.J.; Kerton, F.M.; Jalsa, N.K. Preparation and characterization of biochar derived from the fruit seed of *Cedrela odorata L* and evaluation of its adsorption capacity with methylene blue. *Sustain. Chem. Pharm.* **2021**, 21, 100421.
49. Swan, N.B.; Zaini, M.A.A. Adsorption of malachite green and congo red dyes from water: recent progress and future outlook. *Ecol. Chem. Eng. S.* **2019**, 26, 119–132.
50. Singh, S.; Prajapati, A.K, Chakraborty, J.P.; Mondal, M.K. Adsorption potential of Biochar obtained from pyrolysis of raw and torrefied *Acacia nilotica* towards removal of methylene blue dye from synthetic wastewater. *Biomass Convers. Bior.* **2023**, 13, 6083–6104.